

# Thermodynamics and Dynamics of the Two-Scale Spherically-Symmetric Jagla Model of Anomalous Liquids

Limei Xu<sup>1</sup>, Sergey V. Buldyrev<sup>2,1</sup>, C. Austen Angell<sup>3</sup>, H. Eugene Stanley<sup>1</sup>

<sup>1</sup>*Center for Polymer Studies and Department of Physics, Boston University, Boston, MA 02215 USA*

<sup>2</sup>*Department of Physics, Yeshiva University, 500 West 185th Street, New York, NY 10033 USA*

<sup>3</sup>*Department of Chemistry, Arizona State University, Tempe, Arizona 85287 USA*

(Dated: October 5, 2018 xbas.tex)

Using molecular dynamics simulations, we study a liquid model which consists of particles interacting via a spherically-symmetric two-scale Jagla ramp potential with both repulsive and attractive ramps. The Jagla potential displays anomalies similar to those found in liquid water, namely expansion upon cooling and an increase of diffusivity upon compression, as well as a liquid-liquid (LL) phase transition in the region of the phase diagram accessible to simulations. The LL coexistence line, unlike in tetrahedrally-coordinated liquids, has a positive slope, because of the Clapeyron relation, corresponding to the fact that the high density phase (HDL) is more ordered than low density phase (LDL). When we cool the system at constant pressure above the critical pressure, the hydrodynamic properties rapidly change from those of LDL-like to those of HDL-like upon crossing the Widom line. The temperature dependence of the diffusivity also changes rapidly in the vicinity of the Widom line, namely the slope of the Arrhenius plot sharply increases upon entering the HDL domain. The properties of the glass transition are different in the two phases, suggesting that the less ordered phase (LDL) is fragile, while the more ordered phase (HDL) is strong, which is consistent with the behavior of tetrahedrally-coordinated liquids such as water, silica, silicon, and  $\text{BeF}_2$ .

## I. INTRODUCTION

An open question of general interest concerning liquid water is the relation between a liquid-liquid (LL) phase transition and the dynamic properties [1, 2, 3, 4, 5, 6, 7, 8]. The LL phase transition may have a strong effect on the dynamic properties of supercooled water, including the glass transition [9, 10]. In deeply supercooled states, some glass-formers show “strong” behavior with a well-defined activation energy, while other glass-formers display “fragile” behavior [11]. Water appears to show a crossover between fragile behavior at high T to strong behavior at low T [12, 13, 14, 15, 16]. The recent study on the Stillinger-Weber model of silicon [17], which confirms the LL phase transition, suggests that the less ordered high-density liquid (HDL) is fragile, while the more ordered low-density liquid (LDL) is strong. These authors observed a power-law singularity of the diffusivity in the less ordered HDL phase as it approaches the spinodal of the LL transition at constant pressure. Recently the fragility transition in nano-confined water was studied in neutron scattering experiments pioneered by the Chen group at MIT [3, 4], who found that water appears to show a crossover between non-Arrhenius (“fragile”) behavior at high T to Arrhenius (“strong”) behavior at low T [3, 4, 12, 13]. Their findings were confirmed using NMR by Mallamace *et al.* [6].

A set of realistic water models—ST2, TIP5P, TIP4P, TIP3P, and SPC/E—with progressively decreasing tetrahedrality which bracket the behavior of real water have been studied to explore the generic mechanisms of LL phase transition and anomalies associated with it [1, 2, 5, 18, 19, 20, 21, 22, 23, 24, 25, 26]. Studies [20, 27, 28, 29, 30, 31, 32, 33] show that tetrahedral-

ity is not a necessary condition for anomalous behavior and several spherically-symmetric potentials are indeed able to generate density and/or diffusion anomalies.

In this article, we study a simplified model [Fig. 1] based on spherically-symmetric soft-core potentials with both attractive and repulsive parts [31]. Using extensive molecular dynamics (MD) simulations, we study the static properties, and find that similar to water models, the simple Jagla potential exhibits a density anomaly (TMD), diffusivity anomaly as well as structural anomaly [34]. We further explore the dynamic behavior along different constant pressure paths in HDL (more ordered) and LDL (less ordered) phase. We observe a non-Arrhenius behavior in the less ordered LDL and Arrhenius behavior in the more ordered HDL phase, as well as a dynamic crossover which occurs above the LL critical point as the system is cooled down along constant pressure paths. We put forth a possible interpretation of the dynamic crossover which occurs above the critical point in terms of the LL critical point and its associated Widom line [5]. Thermodynamic response functions—constant pressure specific heat  $C_P$ , constant temperature compressibility  $K_T$  and the structural order parameters,  $Q_6$  (orientational) and  $t$  (translational), support a relation between the dynamic crossover and the LL phase transition.

The outline of the paper is as follows. In Sec. II, we introduce the spherically-symmetric Jagla potential. In Sec. III, we describe the method of the MD simulation. In Sec. IV, we define the quantities which we study. In Sec. V, we investigate the static properties of the model, while Sec. VI contains the simulation results of the dynamic properties. Section VII discusses the relation with water and another tetrahedral liquid  $\text{BeF}_2$ .

## II. SPHERICALLY-SYMMETRIC TWO-SCALE JAGLA RAMP POTENTIAL

A spherically-symmetric potential with two different length scales has been studied [5, 20, 27, 30, 31, 32, 33]. Here, we study the linear ramp potential but with both attractive and repulsive parts [31]. The potential is defined as

$$U(r) = \begin{cases} \infty & r < a \\ U_A + (U_A - U_R)(r - b)/(b - a) & a < r < b, \\ U_A(c - r)/(c - b) & b < r < c, \\ 0 & r > c \end{cases} \quad (1)$$

where  $U_R = 3.5U_0$  is the repulsive energy,  $U_A = -U_0$  is the attractive part,  $a$  is the hardcore diameter,  $b = 1.72a$  is the well minimum, and  $c = 3a$  is the cutoff at large distance [Fig. 1].

## III. METHODS

We apply the discrete MD method [33, 35], approximating the continuous potential Eq. (1) by step functions,

$$U_n(r) = \begin{cases} \infty & r < a \\ U_R - k_1 \Delta U_1 & a + k_1 \Delta r < r < a + (k_1 + 1) \Delta r, \\ U_A & b < r < b', \\ U_A + k \Delta U_2 & b' + (k_2 - 1) \Delta r' < r < b' + k_2 \Delta r', \\ 0 & r > c \end{cases} \quad (2)$$

where  $\Delta r \equiv 0.02a$ ,  $\Delta r' \equiv 0.16a$ ,  $b' = b + 1/2\Delta r'$ ,  $c' = c - 1/2\Delta r'$ ,  $\Delta U_1 = (U_R - U_0)/n_1$  with  $n_1 = 36$ ,  $\Delta U_2 = U_0/n_2$  with  $n_2 = 8$ ,  $0 \leq k_1 \leq n_1 - 1$ , and  $1 \leq k_2 \leq n_2$ .

The standard discrete MD algorithm has been implemented for particles interacting with step potentials [20, 35, 36, 37, 38, 39]. We use  $a$  as the unit of length, particle mass  $m$  as the units of mass, and  $U_0$  as the unit of energy. The simulation time is therefore measured in units of  $a\sqrt{m/U_0}$ , temperature in units of  $U_0/k_B$ , pressure in units of  $U_0/a^3$ , and density  $\rho \equiv Na^3/L^3$ , where  $L$  is the size of the system and  $N = 1728$  is the number of particles.  $NVE$ ,  $NVT$  and  $NPT$  ensembles are applied in our simulation [21, 37].

## IV. THE FOUR QUANTITIES STUDIED

(a) The diffusion coefficient is defined as

$$D \equiv \lim_{t \rightarrow \infty} \frac{\langle [\vec{r}(t' + t) - \vec{r}(t')]^2 \rangle_{t'}}{6t}, \quad (3)$$

where  $\langle \dots \rangle_{t'}$  denotes an average over all particles and over all  $t'$ .

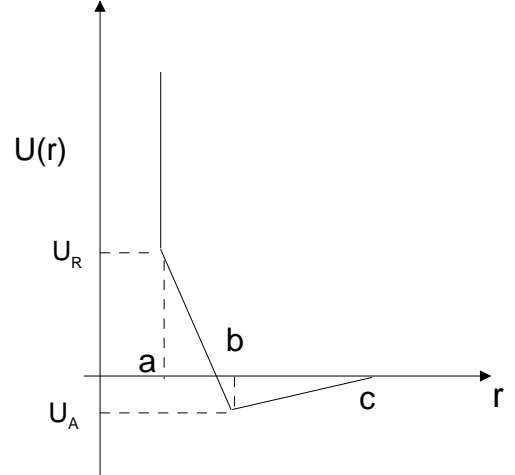


FIG. 1: (a) The spherically-symmetric “two-scale” Jagla ramp potential with attractive and repulsive ramps. Here  $U_R = 3.5U_0$ ,  $U_A = -U_0$ ,  $a$  is the hard core diameter,  $b = 1.72a$  is the soft core diameter, and  $c = 3a$  is the long distance cutoff.

(b) The static structure factor for wave vector  $\vec{q}$  is  $S(\vec{q}) = F(\vec{q}, t = 0)$ , where  $F(\vec{q}, t)$  is the intermediate scattering function defined as

$$F(\vec{q}, t) \equiv \langle \rho(\vec{q}, t) \rho(-\vec{q}, 0) \rangle \quad (4)$$

with the wave vector  $q = 2i\pi/L$ ,  $i = 1, 2, \dots$  and the Fourier transform of the density function

$$\rho(\vec{q}, t) \equiv \sum_j \exp[-i\vec{q} \cdot \vec{r}_j(t)]. \quad (5)$$

(c) The translational order parameter [34, 40]

$$t \equiv \int_0^{r_c} |g(r) - 1| dr \quad (6)$$

where  $r$  is the radial distance,  $g(r)$  is the pair correlation function, and  $r_c = L/2$  is the cutoff distance. A change in the translational order parameter indicates a change in the structure of the system. For uncorrelated systems, the interaction in the system is short-ranged with  $g(r) = 1$ , leading to  $t = 0$ ; for long-range correlated systems, the modulations in  $g(r)$  persist over large distances, causing  $t$  to grow.

(d) The orientational order parameter  $Q$  characterizing the average local order of the system [40] is defined as

$$Q_\ell \equiv \left[ \frac{4\pi}{2\ell + 1} \sum_{m=-\ell}^{m=\ell} |Y_{\ell,m}|^2 \right]^{1/2}, \quad (7)$$

where  $Y_{\ell,m}(\theta, \phi)$  is the spherical harmonic function with  $\theta, \phi$  are angles between the central particle and its 12 nearest neighbors, and  $\ell = 6$ . In general,

the value of  $Q_6$  increases as the local order of a system increases, e.g.  $Q_6=0.574$  for the fcc lattice and  $Q_6 = 0.289$  for uncorrelated systems.

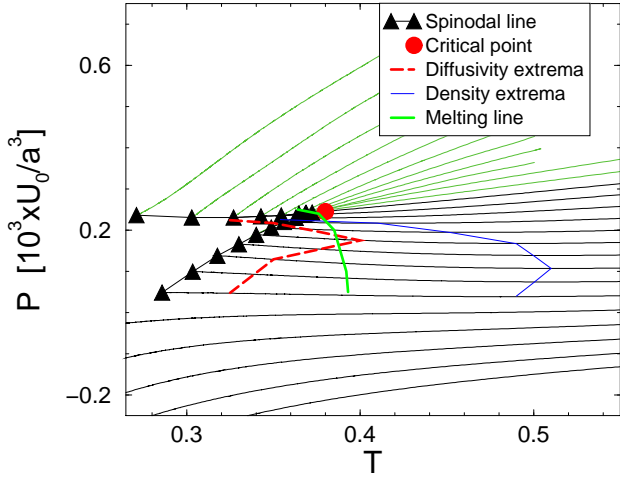


FIG. 2: The equation of state  $P(T, \rho_0)$  of the ramp potential for 26 values of  $\rho_0 \equiv N a^3 / L^3$ , where  $L = 15.0, 15.2, 15.4, \dots, 20.0$  is the cell edge. The LL critical point (closed circle) is located at  $P = 0.243$ , and  $T = 0.37$ , well above the equilibrium melting line (heavy solid curve). The gas-liquid critical point, not shown, is located at much higher temperature  $T_{gl} = 1.446$  ( $P_{gl} = 0.0417$  and  $\rho_{gl} = 0.102$ ). The density anomaly is represented by connecting all the points with  $(\partial \rho / \partial T)_P = 0$ . The locus of the density extrema bounds the region of the diffusivity anomaly.

## V. SIMULATION RESULTS: STATICS

### A. Equation of state

The equation of state of the Jagla model [Fig. 2] is obtained using two steps: (1) constant volume simulation upon slowly cooling (NVT-ensemble), which allows us to obtain the equation of an isochore in a single run; (2) constant energy (NVE-ensemble) simulation of individual state points of a particular interest. The spinodals are defined by the crossing of isochores  $P(T, \rho)$  and  $P(T, \rho + \Delta \rho)$ , where

$$\left( \frac{\partial P}{\partial \rho} \right)_T = 0. \quad (8)$$

The hysteresis of volume [Fig. 3(a)] and enthalpy [Fig. 3(b)] upon compression and decompression along constant temperature  $T = 0.34$ , and the hysteresis of volume [Fig. 3(c)] and enthalpy [Fig. 3(d)] upon heating and cooling along constant pressure paths are consistent with the existence of a LL phase transition. The LL critical point, with  $T_c = 0.375$ ,  $P_c = 0.243$  and  $\rho_c = 0.37$ , is located at the maximal temperature on the

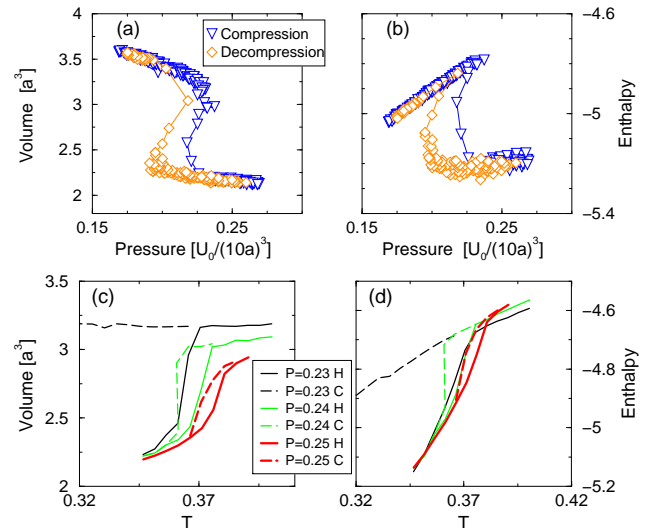


FIG. 3: Hysteresis upon compression and decompression along a constant temperature path with  $T = 0.34$ : (a) Volume per particle and (b) Enthalpy per particle. Hysteresis upon cooling (C) and heating (H) along constant pressure paths: (c) Volume per particle and (d) Enthalpy per particle.

spinodals. The coexistence line, obtained by the Maxwell rule by integrating the isotherms, has a positive slope of  $0.96 \pm 0.02 k_B a^{-3}$ .

According to the Clapeyron equation

$$\frac{dP}{dT} = \frac{\Delta S}{\Delta V}, \quad (9)$$

the entropy in the HDL phase is lower than the entropy in the LDL phase. Hence, the HDL phase is more ordered than the LDL phase, which is the opposite of the LL transition found in simulations for water [2] and silicon [15].

We also studied the spontaneous liquid-liquid phase transition using *NPT* ensemble [Fig. 4]. Simulations of the isobaric heating of the HDL liquid below the critical point show that the HDL phase loses its stability and spontaneously changes into the LDL in the vicinity of the HDL spinodal line [Fig. 4]. The LL critical point of the Jagla model, in contrast to those of water and silicon models, lies well above the equilibrium melting line [Fig. 2] at which the solid and liquid phases coexist and are in equilibrium.

Very recently, Gibson and Wilding [41] study the family of Jagla potentials with decreasing soft-core distance and found that there is a parameter range within which the critical point lies below the crystallization line, and the coexistence line has a negative slope, resembling the situation for water.

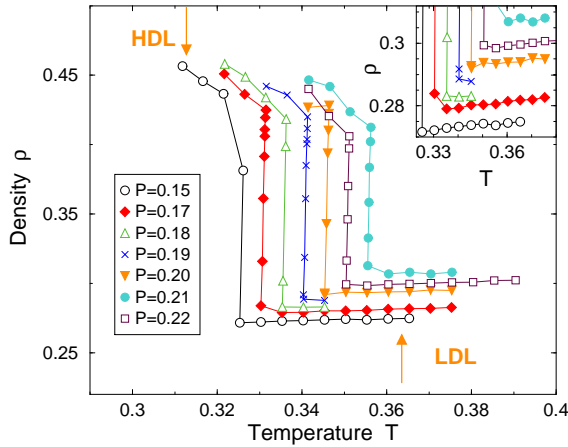


FIG. 4: Liquid – liquid phase transition. Upon heating along constant pressure paths below the critical point, the system experience a HDL to LDL phase transition near the HDL spinodal line. The inset shows the density anomaly upon heating along constant pressure paths.

### B. Density Anomaly

The temperature of maximum density (TMD) line is defined by  $(\partial V/\partial T)_P = 0$ . Due to the general thermodynamic relation

$$\left(\frac{\partial V}{\partial T}\right)_P = - \left(\frac{\partial P}{\partial T}\right)_V \left(\frac{\partial V}{\partial P}\right)_T, \quad (10)$$

the TMD line coincides with the locus of points satisfying  $(\partial P/\partial T)_V = 0$ , which defines the pressure minimum on each isochore (Fig. 2). The density anomaly (density increase upon heating along constant pressure paths) can also be seen in the inset of Fig. 4.

### C. Thermodynamics

A sketch of the phase diagram based on the equation of state [Fig. 2] is shown in Fig. 5(a) and the simulated phase diagram is shown in Fig. 5(b). Different thermodynamic response functions such as  $C_P$  and  $K_T$ , which diverge at the critical point, have maxima at temperatures  $T_{\max}(P)$ , which can be regarded as temperatures on the extension of the coexistence line above the critical temperature (the Widom line[5]) as we cool the system at constant pressure  $P_0 > P_c$  [42, 43, 44, 45]. We investigate  $C_P$  and  $K_T$  in the Jagla model along paths  $\alpha$  and path  $\beta$  (Fig. 5). We find that, along paths  $\alpha$ ,  $C_P$  has a maximum at  $T_{\max}(P_0)$  [Fig. 6(a)], while  $K_T$  has a maximum at a slightly different  $T_{\max}(P_0)$  [Fig. 6(b)]. The response functions— $C_P$  and  $K_T$ —increase continuously along path  $\beta$  [Fig. 5(a)] before the system reaches the stability limit near the LDL spinodal [18].

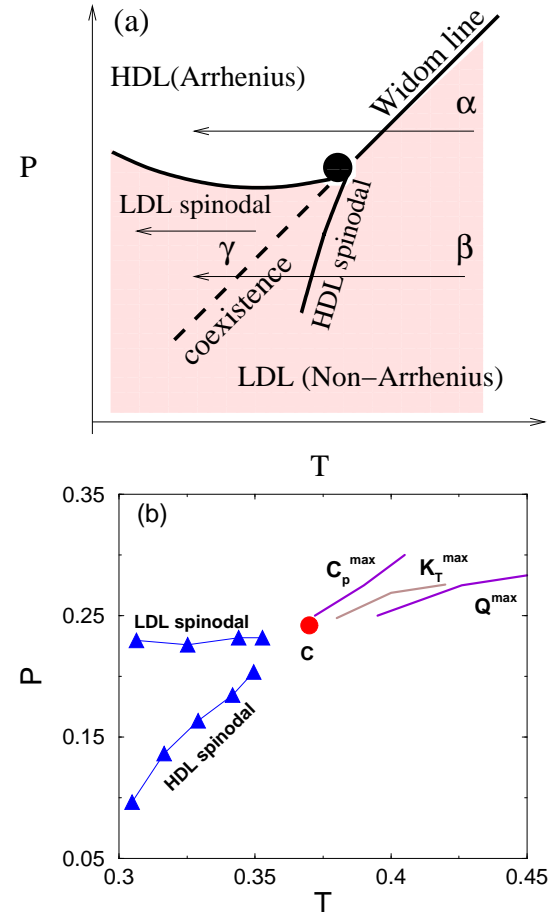


FIG. 5: A sketch of the  $P-T$  phase diagram for the two-scale Jagla model. We study three different paths in the vicinity of the LL critical point: (i)  $P_0 > P_c$  (path  $\alpha$ ). Upon cooling along path  $\alpha$ , the liquid changes from a low density state (characterized by a non-Arrhenius dynamic behavior) to a high density state (characterized by Arrhenius dynamic behavior) as the path crosses the Widom line. (ii)  $P_0 < P_c$  (path  $\beta$ ). Upon cooling along path  $\beta$ , the liquid remains in the LDL phase as long as path  $\beta$  does not cross the LDL spinodal line. Thus one does not expect any dramatic change in the dynamic behavior along the path  $\beta$ . (iii)  $P_0 < P_c$  (path  $\gamma$ ). Upon cooling along path  $\gamma$ , the liquid remains in HDL phase. Its dynamics, different from that of the LDL phase, follows Arrhenius behavior. (b) The  $P-T$  phase diagram for the two-scale Jagla model. The loci of the specific heat maximum  $C_P^{\max}$ , the compressibility maximum  $K_T^{\max}$ , and orientational order parameter maximum  $Q^{\max}$  are similar but not quite identical.

### D. Structural order

Analogously, we can expect that the structural properties of the system also change from those resembling the LDL phase to those resembling the HDL phase when the system crosses the Widom line (the extension of the coexistence line). The pair correlation function  $g(r)$  for different  $T$  along a constant pressure path is shown in

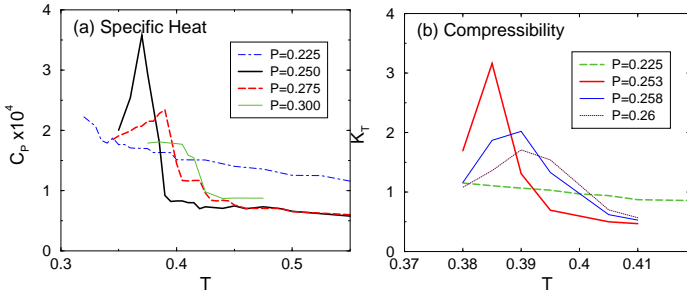


FIG. 6: Response functions for the Jagla model as function of temperature for different values of  $P_0 > P_c$  [Fig. 5, path  $\alpha$ ]. (a) Constant pressure specific heat  $C_P$  and (b) constant temperature compressibility  $K_T$ . Both  $C_P$  and  $K_T$  have maxima, as is known to occur experimentally [42, 49]. For large  $P_0$  the peaks become less pronounced and shift to higher temperature as the system is farther away from the LL critical point.

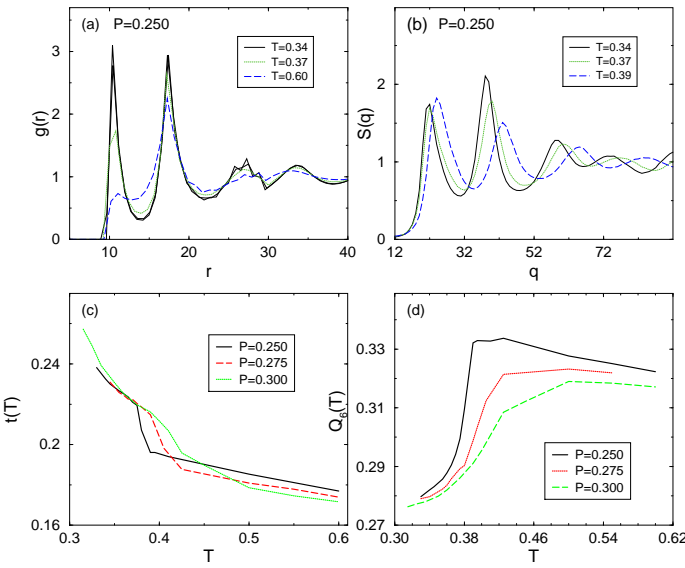


FIG. 7: (a) The pair correlation function  $g(r)$  at constant pressure  $P_0 = 0.250$ . The magnitude of the first peak indicates a HDL-like liquid at low  $T$  and LDL-like liquid at high  $T$ . (b) Distribution of  $q$  vectors at constant pressure  $P_0 = 0.250$ . The shifts of the first and second peaks in the distribution of the  $q$  vectors further indicates that the liquid changes smoothly from HDL-like to LDL-like as it crosses the Widom line. (c) The translational order parameter  $t$  and (d) the orientational order parameter  $Q_6$  along constant pressure paths.

Fig. 7(a). At low temperature  $g(r)$  exhibits a more pronounced first peak near the hard core distance and a less pronounced peak at high  $T$ , indicating a change from the LDL-like structure to HDL-like structure upon cooling along paths  $\alpha$ . The same behavior can also be seen from the static structure factor  $S(q)$  [Fig. 7(b)]. The sharp transition in the translational order parameter  $t$  [Fig. 7(c)] and the peaks in the orientational order pa-

rameter  $Q_6$  [Fig. 7(d)] above the LL critical point along path  $\alpha$ , indicate that as the system crosses the Widom line region [Fig. 5(b)], the local structure of the system also changes from LDL-like side to HDL-like side, which is consistent with the features observed in the thermodynamic response functions.

## VI. SIMULATION RESULTS: DYNAMICS

### A. Diffusivity Anomaly

Figure 8 shows the diffusivity  $D(\rho)$  along seven isotherms. There exists a diffusivity anomaly region along each isotherm where the diffusivity *increases* upon compressing instead of decreasing. The loci of the diffusivity extrema where  $(\partial D/\partial P)_T = 0$  [heavy dashed lines in Fig. 2 and Fig. 8] defines the diffusivity anomaly region.

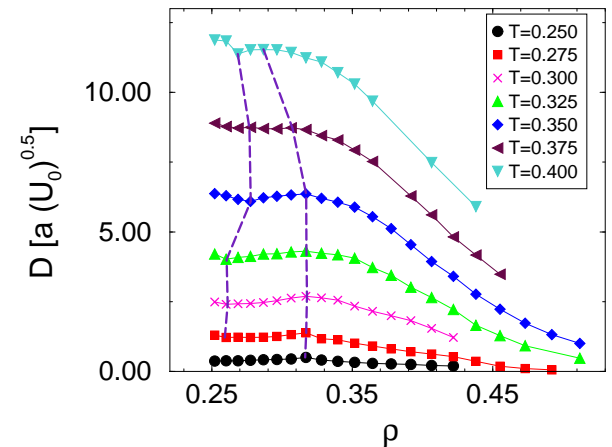


FIG. 8: Diffusivity as a function of density for seven values of temperature. The diffusivity anomaly region, where  $D$  increases with compression (density), is located within the diffusivity extrema lines (heavy dashed line).

We study the  $T$  dependence of  $D$  along three different constant pressure paths [Fig. 5(a)]:

- Path  $\alpha$ ,  $P_0 > P_c$  (one-phase region);
- Path  $\beta$ ,  $P_0 < P_c$  (in the LDL phase); and
- Path  $\gamma$ ,  $P_0 < P_c$  (in the HDL phase).

### B. Dynamics for $P < P_c$

For  $P_0 < P_c$ , the diffusivity  $D$  at high temperature  $T > T_c$  follows the Arrhenius law

$$D = D_0 \exp \left( -\frac{E_A}{k_B T} \right) \quad (11)$$

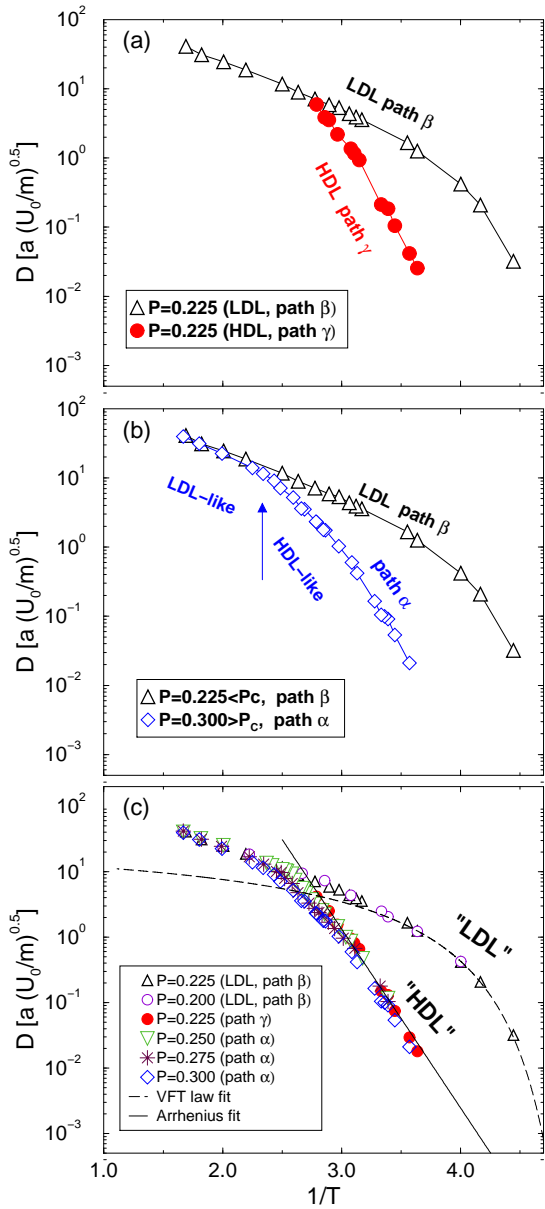


FIG. 9: Dynamic behavior for Jagla potential. The  $T$ -dependence of diffusivity  $D$  along constant pressure paths: (a)  $P_0 = 0.225 < P_c$  for both path  $\beta$  and path  $\gamma$ . The more ordered phase (HDL) is strong, while the less ordered phase (LDL) is fragile. (b) Path  $\beta$  with  $P_0 = 0.225 < P_c$ , and path  $\alpha$  with  $P_0 = 0.300 > P_c$ . A dynamic crossover occurs along constant pressure paths above the critical pressure when the Widom line is crossed [Fig. 6]. (c) Path  $\beta$  with  $P_0 = 0.200$ ,  $P_0 = 0.225 < P_c$ , path  $\gamma$  with  $P_0 = 0.225 < P_c$ , and path  $\alpha$  with  $P_0 = 0.250, 0.300 > P_c$  [Fig. 5].

with a roughly pressure independent activation energy  $E_A \approx 1.53$ , while at low temperatures in the two-phase region,  $D$  behaves differently along path  $\beta$  and path  $\gamma$  upon cooling at constant pressure [Fig. 9]. Along path  $\beta$  [Fig. 5(a)] which belongs to the LDL phase, the  $T$  dependence of  $D$  is non-Arrhenius and follows the Vogel-

Fulcher-Tamann law

$$D = D_0 \exp\left(-\frac{B}{T - T_0}\right) \sim D_0 \exp\left(-\frac{T_0}{T - T_0} \frac{1}{f}\right). \quad (12)$$

For  $P = 0.225$  the fitting parameters are  $B \approx 0.2$ ,  $T_0 \approx 0.184$ , and the fragility parameter  $f = T_0/B \approx 0.66$  [Fig. 9]. Quantitatively, the “steepness index of the fragility” [46]  $m \approx 368$ , with the glass temperature  $T_g \approx 0.192$  estimated as the temperature at which  $\exp(B/(T - T_0)) = 10^k$ , where  $k = 16$  is a typical value for thermally-activated systems [46]. The large value of  $m$  indicates that the behavior in the LDL phase resembles that of a very fragile liquid. Note that the value of the index number  $m$  largely depends on the Vogel-Fulcher-Tamman fitting at the last data point [Fig. 9(a)].

On the other hand, along paths  $\gamma$  which belong to the HDL phase,  $D$  follows Arrhenius behavior with  $E_a \approx 6.30$ , which is much larger than the activation energy at high temperature.

### C. Dynamics for $P > P_c$

For  $P_0 > P_c$  along path  $\alpha$ , there is a crossover in the behavior of  $D$  near  $T \approx 0.4$  [Figs. 9(b) and 9(c)]. Such a crossover, where  $C_P$  passes through a maximum [Fig. 6(a)], would be predicted by the Adam-Gibbs equation [16, 47],

$$D = D \exp\left(-\frac{C}{TS_c}\right), \quad (13)$$

because of the rapid change in the temperature dependence on  $S_c$  as the Widom line is crossed. When  $C_P$  has fallen to a smaller and more slowly changing value, the temperature dependence of  $D$  assumes an Arrhenius behavior but with a somewhat larger slope than at high temperatures where Fig. 6(a) shows  $C_P$  to be very small. The behavior is similar to what was observed in experimental studies of the strong liquid  $\text{BeF}_2$  [48] and in simulations of  $\text{SiO}_2$  [15]. In fact, the parallel with the case of  $\text{BeF}_2$  [48] is remarkable. In each case the Arrhenius slope extrapolates to an intercept at  $1/T = 0$ , which is six orders of magnitude above the intercept of the high temperature Arrhenius part of the plot (which is common to all phases). Thus, the behavior of the HDL-like liquid on the low-temperature side of the Widom line can be classified as that of a strong liquid. The behavior on the high-temperature side of the Widom line, in the LDL-like phase, however, is very different, resembling that of the fragile liquid (LDL-like), as is clear from Figs. 9(b) and 9(c). Thus, the present spherically-symmetric Jagla ramp potential exhibits a dynamic crossover from LDL-like (fragile liquid) at high-temperature to HDL-like (strong liquid) at low-temperature, suggesting the analogous fragile-to-strong transition as in water, with the difference that the strong liquid is now the HDL phase.

## VII. DISCUSSION

### A. Jagla Ramp Potential

The mechanisms underlying the different dynamic behaviors we find can be related to the LL phase transition [Fig. 5(a)]. The coexistence line has a positive slope, so we have one phase for  $P > P_c$  and two phases—LDL and HDL—for  $P < P_c$ . According to the Clapeyron equation, HDL entropy is lower than LDL entropy, so HDL is more ordered than LDL which is the opposite of water. In the region of the P-T phase diagram between the LDL and HDL spinodals, the system can exist in both the LDL and HDL phases, one stable and one metastable.

- (i) The limit of stability of the less-ordered LDL phase is determined by the high pressure LDL spinodal  $P_{\text{LDL}}(T)$ , which, for our model, is unlikely to be crossed by cooling the system at constant pressure [Figs. 3(c) and (d)]—because  $P_{\text{LDL}}(T) \approx P_c$  for all  $T$  except in the immediate vicinity of the liquid-liquid critical point [Fig. 5]. The dynamic behavior of the less ordered LDL phase is non-Arrhenius, which is the characteristic of fragile glass formers [Fig. 5].
- (ii) On the other hand, the limit of stability of the more ordered HDL phase is determined by the low pressure HDL spinodal  $T_{\text{HDL}}(P)$  [Fig. 5], which can be crossed by heating the HDL phase at constant pressure [Fig. 3(c) and (d)]. That is why the dynamic behavior of the more ordered HDL phase can be studied only when  $T < T_{\text{HDL}}(P)$  for  $P < P_c$ .

### B. Comparison with Water

For the Jagla model, the dynamic crossover upon cooling for  $P_0 > P_c$  (Path  $\alpha$ ) is the same that was observed in realistic water models [3, 13], which is a fragile to strong transition. In water models which have a negatively sloped coexistence, the density of the high temperature phase is larger than the density of the low temperature phase [Fig. 10]. The density of the high temperature phase is larger than the density of the low temperature phase if the coexistence line has a negative slope, so the high temperature less ordered phase is the HDL phase. When water is cooled at  $P_0 > P_c$  [Fig. 10, path  $\beta$ ], it crosses the coexistence line but does not cross the spinodal of the less ordered HDL phase, which may become almost horizontal line on the  $P-T$  plane as recent ST2 simulations suggest [2]. Thus, water remains in the metastable HDL phase even at very low temperatures, since the low-density phase may not nucleate out of the HDL phase. Accordingly, above the critical pressure, water may remain fragile even at very low temperatures. In contrast, upon cooling at  $P_0 < P_c$  [Fig. 10, path  $\alpha$ ], water crosses the Widom line, and its thermodynamic properties continuously change from those of the HDL phase

to those of the LDL phase. This is demonstrated by the  $C_P$  peak found by cooling water in small pores at atmospheric pressure [49]. Therefore, for  $P_0 < P_c$  one expects a fragile-to-strong transition upon cooling, which is indeed experimentally observed [3, 4].

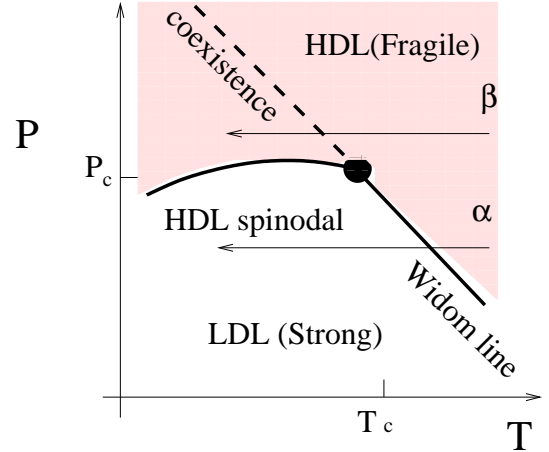


FIG. 10: A sketch of the  $P-T$  phase diagram for water models, showing paths  $\alpha$  and  $\beta$ . Note that unlike the Jagla two-scale ramp potential [Fig. 5(a)], the HDL is less ordered than the LDL, so by the Clapeyron relation, the Widom line has negative slope.

### C. Comparison with the Tetrahedral Liquid $\text{BeF}_2$

Interestingly, what was observed in a combined MD/experimental study of  $\text{BeF}_2$  [48, 50, 51] show a dynamic crossover similar to what we observed for Jagla model for  $P_0 > P_c$  [Fig. 9(a)]. In addition, the MD simulations of  $\text{BeF}_2$  show a density anomaly and specific heat maximum close to the point of the dynamic crossover at about  $2T_g$ . In the Jagla model, the dynamic crossover and the  $C_P$  maximum occur at higher temperatures  $T \approx 3.5T_g$ . The difference between  $\text{BeF}_2$  and the Jagla model is that a second LL critical point has not been directly observed for  $\text{BeF}_2$ . Therefore, we can not call the region of fast change of the dynamic and thermodynamic properties a Widom line. However, the extrapolation of the simulation isochores in the density anomaly region suggests possible existence of a critical point at lower temperature and higher pressure. Thus, the region of fast changes of the thermodynamic response functions is possibly associated with a Widom line emanating from the hypothetical critical point [52, 53] hidden in the inaccessible region. As in water, this region in  $\text{BeF}_2$  has negative slope, suggesting that the dynamic crossover in  $\text{BeF}_2$  upon cooling is related to the entropy decrease from HDL-like on the high-temperature side to LDL-like on the low-temperature side.

### VIII. SUMMARY

In summary, we systematically study a simple spherically-symmetric two-scale Jagla potential with both repulsive and attractive parts. We find a LL phase transition in an accessible region of the P-T phase diagram. The Jagla potential also displays water-type thermodynamic and dynamic anomalies, as well as a dynamic crossover which occurs as the system crosses the Widom line while cooled along constant pressure paths  $P > P_c$ . Our simulations, similar to simulations of silicon [17], show that the dynamics is Arrhenius in the more ordered phase (HDL for Jagla model) and fragile for the less ordered phase (LDL for Jagla model). Our study shows that the dynamics is Arrhenius on the low-temperature side and fragile on the high-temperature side, as in water. The dynamic crossover for  $P > P_c$  is consistent with

(i) the experimental observation in confined geometries (small pores) of a fragility transition [3], and (ii) experimental observation of a peak in the specific heat upon cooling water at atmospheric pressure in nanopores [49].

### Acknowledgments

We thank S.-H Chen, D. Chandler, P. G. Debenedetti, G. Franzese, J. P. Garrahan, P. Kumar, J. M. H. Levelt Sengers, M. Mazza, P. H. Poole, F. Sciortino, S. Sastry, F. W. Starr, B. Widom, and Z. Yan for helpful discussions and NSF grant CHE 0096892 for support. We also thank the Boston University Computation Center for allocation of CPU time. SVB thanks the Office of the Academic Affairs of Yeshiva University for funding the high-performance computer cluster.

---

[1] P. H. Poole, F. Sciortino, U. Essmann, and H. E. Stanley, *Nature (London)* **360**, 324 (1992); P. H. Poole, F. Sciortino, U. Essmann, and H. E. Stanley, *Phys. Rev. E* **48**, 3799 (1993); P. H. Poole, U. Essmann, F. Sciortino, and H. E. Stanley, *Phys. Rev. E* **48**, 4605 (1993); F. Sciortino, P. H. Poole, U. Essmann and H. E. Stanley, *Phys. Rev. E* **55**, 727 (1997); O. Mishima and H. E. Stanley, *Nature* **396**, 329 (1998).

[2] P. H. Poole, F. Sciortino, T. Grande, H. E. Stanley, and C. A. Angell, *Phys. Rev. Lett.* **73**, 1632 (1994).

[3] A. Faraone, L. Liu, C.-Y. Mou, C.-W. Yen, and S.-H. Chen, *J. Chem. Phys.* **121**, 10843 (2004).

[4] L. Liu, S.-H. Chen, A. Faraone, C.-W. Yen, and C.-Y. Mou, *Phys. Rev. Lett.* **95**, 117802 (2005).

[5] L. Xu, P. Kumar, S. V. Buldyrev, S.-H. Chen, P. Poole, F. Sciortino, and H. E. Stanley, *Proc. Natl. Acad. Sci. USA* **102**, 16807 (2005); L. Xu, E. Issac, S. V. Buldyrev, and H. E. Stanley, *J. Phys.: condens. Matter* (in press); P. Kumar, S. V. Buldyrev, and H. E. Stanley, *Proc. NATO ARW, Odessa, Oct 2005* (in press).

[6] F. M. Mallamace, M. Broccio, C. Corsaro, A. Faraone, U. Wanderlingh, L. Liu, C.-Y. Mou, and S.-H. Chen, *J. Chem. Phys.* **124**, xxxx (2006).

[7] S.-H. Chen, L. Liu, E. Fratini, P. Baglioni, A. Faraone, and E. Mamontov, *Proc. Natl. Acad. Sci USA* (in press).

[8] P. Kumar, L. Xu, Z. Yan, M. G. Mazza, S. V. Buldyrev, S.-H. Chen, S. Sastry, and H. E. Stanley, *cond-mat/0603557*.

[9] V. Velikov, S. Borick, and C.A. Angell, *Science* **294**, 2335 (2001).

[10] G. P. Johari, *J. Chem. Phys. B* **107**, 9063 (2003).

[11] C. A. Angell, *Science* **267**, 1924 (1995).

[12] C. A. Angell, *J. Phys. Chem.* **97**, 6339 (1993).

[13] K. Ito, C. T. Moynihan, and C. A. Angell, *Nature* **398**, 492 (1999).

[14] R. Bergman and J. Swenson, *Nature* **403**, 283 (2000).

[15] I. Saika-Voivod, P. H. Poole, and F. Sciortino, *Nature* **412**, 514 (2001).

[16] F. W. Starr, C. A. Angell, and H. E. Stanley, *Physica A* **323**, 51 (2003).

[17] S. Sastry and C. A. Angell, *Nature Materials* **2**, 739 (2003).

[18] P. G. Debenedetti, *Metastable Liquids: Concepts and Principles* (Princeton University Press, Princeton, 1996).

[19] O. Mishima and H. E. Stanley, *Nature* **392**, 164 (1998).

[20] G. Franzese, G. Malescio, A. Skibinsky, S. V. Buldyrev, and H. E. Stanley, *Nature* **409**, 692 (2001).

[21] M. Yamada, S. Mossa, H. E. Stanley, F. Sciortino, *Phys. Rev. Lett.* **88**, 195701 (2002).

[22] P. G. Debenedetti, *J. Phys.: Condens. Matter* **15**, R1669 (2003); P. G. Debenedetti and H. E. Stanley, *Physics Today* **56**[issue 6], 40 (2003).

[23] F. Sciortino, E. La Nave, and P. Tartaglia, *Phys. Rev. Lett.* **91**, 155701 (2003).

[24] D. Paschek, *Phys. Rev. Lett.* **94**, 217802 (2005).

[25] P. H. Poole, I. Saika-Voivod, and F. Sciortino, *J. Phys. Condens. Matter* **17**, L431 (2005).

[26] P. Kumar, S. V. Buldyrev, F. Starr, N. Giovambattista, and H. E. Stanley, *Phys. Rev. E* **72**, 051503 (2005).

[27] P. C. Hemmer and G. Stell, *Phys. Rev. Lett.* **24**, 1284 (1970); G. Stell and P. C. Hemmer, *J. Chem. Phys.* **56**, 4274 (1972); J. M. Kincaid and G. Stell, *J. Chem. Phys.* **67**, 420 (1977); J. M. Kincaid, G. Stell and E. Goldmark, *J. Chem. Phys.* **65**, 2172 (1976); J. M. Kincaid, G. Stell and C. K. Hall, *J. Chem. Phys.* **65**, 2161 (1976).

[28] F. H. Stillinger, *Chem. Phys.* **65**, 3968 (1976).

[29] F. H. Stillinger and D. K. Stillinger, *Physica A* **244**, 358 (1997).

[30] M. R. Sadr-Lahijany, A. Scala, S. V. Buldyrev, and H. E. Stanley, *Phys. Rev. Lett.* **81**, 4895 (1998); *Phys. Rev. E* **60**, 6714 (1999).

[31] E. A. Jagla, *J. Chem. Phys.* **111**, 8980 (1999); *J. Phys. Chem.* **11**, 10251 (1999); *Phys. Rev. E* **63**, 061509 (2001).

[32] A. Scala, M. Reza Sadr-Lahijany, N. Giovambattista, S. V. Buldyrev, and H. E. Stanley, *J. Stat. Phys.* **100** 97 (2000); *Phys. Rev. E* **63** 041202 (2001).

[33] S. V. Buldyrev, G. Franzese, N. Giovambattista, G. Malescio, M. R. Sadr-Lahijany, A. Scala, A. Skibinsky, and H. E. Stanley, in *New Kinds of Phase Transitions: Transformations in Disordered Substances*, NATO Advanced Research Workshop, Volga River, edited by V. Brazhkin, S. V. Buldyrev, V. Ryzhov, and H. E. Stanley

(Kluwer, Dordrecht, 2002), pp. 97–120.

[34] J. R. Errington and P. G. Debenedetti, *Nature* (London) **409**, 318 (2001).

[35] P. Kumar, S. V. Buldyrev, F. Sciortino, E. Zaccarelli, and H. E. Stanley, *Phys. Rev. E* **72**, 021501 (2005).

[36] D. C. Rapaport, *The Art of Molecular Dynamics Simulation* (Cambridge University Press, Cambridge, 1995).

[37] S. V. Buldyrev and H. E. Stanley, *Physica A* **330**, 124 (2003).

[38] G. Franzese, M. I. Marqués, and H. E. Stanley, *Phys. Rev. E* **67**, 011103 (2003); A. Skibinsky, S. V. Buldyrev, G. Franzese, G. Malescio, and H. E. Stanley, *Phys. Rev. E* **69**, 061206 (2004); G. Malescio, G. Franzese, A. Skibinsky, S. V. Buldyrev and H. E. Stanley, *Phys. Rev E* **71**, 061504 (2005).

[39] S. V. Buldyrev, G. Franzese, N. Giovambattista, G. Malescio, M. R. Sadr-Lahijany, A. Scala, A. Skibinsky, and H. E. Stanley, *Physica A* **304**, 23 (2002).

[40] Z. Yan, S. V. Buldyrev, N. Giovambattista, and H. E. Stanley, *Phys. Rev. Lett.* **95**, 130604 (2005); Z. Yan, S. V. Buldyrev, N. Giovambattista, P. G. Debenedetti, and H. E. Stanley, *Phys. Rev. E* (in press), cond-mat/0601554.

[41] H. M. Gibson and N. B. Wilding, cond-mat/0601474 (2006).

[42] M. A. Anisimov, J. V. Sengers, and J. M. H. Levent Sengers, in *Aqueous System at Elevated Temperatures and Pressures: Physical Chemistry in Water, Stream and Hydrothermal Solutions*, edited by D. A. Palmer, R. Fernandez-Prini, and A. H. Harvey (Elsevier, Amsterdam, 2004).

[43] J. M. H. Levent, *Measurements of the compressibility of argon in the gaseous and liquid phase*, Ph.D. Thesis (University of Amsterdam, Van Gorkum & Co., Assen 1958).

[44] A. Michels, J. M. H. Levent, and G. Wolkers, *Physica* **24**, 769 (1958).

[45] A. Michels, J. M. H. Levent, and W. de Graaff, *Physica* **24**, 659 (1958).

[46] The parameter  $m$  is defined in R. Böhmer, K. L. Ngai, C. A. Angell, and D. J. Plazek, *J. Chem. Phys.* **99**, 4201 (1993).

[47] G. Adam and J. H. Gibbs, *J. Chem. Phys.* **43**, 139 (1965).

[48] M. Hemmati, C. T. Moynihan, and C. A. Angell, *J. Chem. Phys.* **115**, 6663 (2001).

[49] S. Maruyama, K. Wakabayashi, and M. Oguni, *AIP Conf. Proc.* **708**, 675 (2004).

[50] S. V. Nemilov, G. T. Petrovskii, and L. A. Krylova, *Inorg. Mater. (Transl. of Neorg. Mater.)* **4**, 1453 (1968).

[51] C. T. Moynihan and S. Cantor, *J. Chem. Phys.* **48**, 115 (1968).

[52] V. V. Brazhkin, A. G. Lyapin, S. V. Popova, and R. N. Voloshin, in *New Kinds of Phase Transitions: Transformations in Disordered Substances*, NATO Advanced Research Workshop, Volga River, edited by V. Brazhkin, S. V. Buldyrev, V. Ryzhov, and H. E. Stanley (Kluwer, Dordrecht, 2002), pp. 15–28.

[53] V. V. Brazhkin, R. N. Voloshin, S. V. Popova, and A. G. Lyapin, in *New Kinds of Phase Transitions: Transformations in Disordered Substances*, NATO Advanced Research Workshop, Volga River, edited by V. Brazhkin, S. V. Buldyrev, V. Ryzhov, and H. E. Stanley (Kluwer, Dordrecht, 2002), pp. 239–254.